Journal of Alloys and Compounds 509 (2011) 5008–5011

Contents lists available at ScienceDirect

Journal of Alloys and Compounds

journal homepage: www.elsevier.com/locate/jallcom

Tunable room temperature ferromagnetism in $Sn_{0.93}Fe_{0.05}M_{0.02}O_{2-\sigma}$ (M = Sb/Mg): The role of electron- and hole-doping

C. Ke[a], W. Zhu[a,*], J.S. Pan[b], Z. Yang[a], Z.P. Li[c], L. Wang[d]

[a] Microelectronics Centre, School of Electrical and Electronic Engineering, Nanyang Technological University, Singapore 639798, Singapore
[b] Institute of Materials Research & Engineering, A*STAR (Agency for Science, Technology and Research), 3 Research Link, Singapore 117602, Singapore
[c] School of Material Science and Engineering, Nanyang Technological University, Singapore 639798, Singapore
[d] School of Physical and Mathematical Science, Nanyang Technological University, Singapore 639798, Singapore

ARTICLE INFO

Article history:
Received 10 November 2010
Received in revised form 28 January 2011
Accepted 31 January 2011
Available online 1 March 2011

Keywords:
Magnetism
Diluted magnetic semiconductor
Tin oxide
X-ray photoemission spectroscopy

ABSTRACT

Bulk polycrystalline $Sn_{0.95}Fe_{0.05}O_{2-\sigma}$ and $Sn_{0.93}Fe_{0.05}M_{0.02}O_{2-\sigma}$ (M = Sb/Mg) samples were fabricated. Detailed X-ray diffraction and transmission electron microscopy analyses revealed that the dopants most probably replaced the Sn in SnO_2 structure, instead of forming impurity phase or nanocluster. By varying the dopant M (Sb/Mg), the electron- (Sb) and hole- (Mg) doping effect on the magnetic properties of $Sn_{0.93}Fe_{0.05}M_{0.02}O_{2-\sigma}$ was investigated. Compared with $Sn_{0.95}Fe_{0.05}O_{2-\sigma}$, the saturation magnetization decreased after doping with Sb and increased after doping with Mg. The changes of Fe oxidation state and carrier type, discovered from X-ray photoelectron spectroscopy, are believed to be responsible for the co-doping tuned ferromagnetism in $Sn_{0.93}Fe_{0.05}M_{0.02}O_{2-\sigma}$.

1. Introduction

Based on the demand of miniaturization in the semiconductor industry, the feature size of silicon-based devices is approaching its physical limit where macroscopic scale law breaks. To overcome such difficulty, researchers never cease to explore multifunctional materials and more sophisticated technologies. Recently, the emerging technology of dilute magnetic semiconductor (DMS) has attracted intensive interest due to its interesting properties and promising applications in spintronics [1–3]. In the DMS-based materials, an additional degree of freedom of the electron (spin) can be realized by doping ferromagnetic 3d transition metals, i.e., Fe, Co, Mn, etc. Various transition-metal-doped systems such as Ge, GaAs, TiO_2, SnO_2 and ZnO have been reported to show robust ferromagnetic response [4–10]. Specifically, room temperature ferromagnetism (RTFM), which favors the device applications, has been achieved in several wide bandgap metal oxides, e.g., TiO_2, SnO_2, ZnO and In_2O_3. Combined with nanotechnology, the magnetic properties of DMS in the form of different nanostructures have also been investigated [11–13]. However, the origin of ferromagnetism in DMS is still controversial, due to the complicated defect states, grain boundary effect, possible secondary magnetic phases and special role of oxygen non-stoichiometry in oxide based DMS [1,14–18]. By varying the electron doping concentration and controlling the density of oxygen vacancy (V_O), Li et al. [19] reported that the RTFM in bulk polycrystalline $(In_{0.85-x}Sn_xFe_{0.15})_2O_3$ is directly related to the V_O. Similar oxygen non-stoichiometry related ferromagnetism in $Sn_{0.95}Fe_{0.05}O_2$ was also observed by Thurber et al. [20] by annealing the sample under controlled atmosphere with varied oxygen concentrations. In addition, compared with electron-doping, hole-doping was found to be more effective in stabilizing the ferromagnetism in ZnO based DMS, according to the theoretical calculations and experimental results [21,22].

In this paper, we investigated the effects of both electron- and hole-doping on the ferromagnetic properties of $Sn_{0.93}Fe_{0.05}M_{0.02}O_{2-\sigma}$ by varying the dopant M (Sb/Mg). A prominent decrease of saturation magnetization (M_s) was observed in $Sn_{0.93}Fe_{0.05}Sb_{0.02}O_{2-\sigma}$. On the contrary, the M_s was significantly enhanced in the case of Mg doping. Based on the results of X-ray photoelectron spectroscopy (XPS) characterization, this co-doping tuned ferromagnetism in $Sn_{0.93}Fe_{0.05}M_{0.02}O_{2-\sigma}$ is attributed to the transition of Fe oxidation state and the change of carrier type.

2. Experimental

SnO_2, as a host material in this study, is a wide bandgap (~3.6 eV) oxide semiconductor with rutile structure. Fe is selected as the magnetic dopant due to its high solid solubility in SnO_2 (up to 10%) [23]. Sb and Mg are chosen to be the electron-

* Corresponding author.
E-mail address: zhuweiguang.ntu@gmail.com (W. Zhu).

0925-8388/$ – see front matter © 2011 Elsevier B.V. All rights reserved.
doi:10.1016/j.jallcom.2011.01.211

and hole-dopant, respectively, based on the following defect equations:

$$Sb_2O_5 \xrightarrow{2SnO_2} 2Sb_{Sn}^{\bullet} + \tfrac{1}{2}O_2(g)\uparrow + 4O_O^{\times} + 2e' \quad (1)$$

$$MgO + \tfrac{1}{2}O_2 \xrightarrow{SnO_2} Mg''_{Sn} + 2O_O^{\times} + 2h^{\bullet} \quad (2)$$

Three bulk polycrystalline samples, $Sn_{0.95}Fe_{0.05}O_{2-\sigma}$ (Fe5), $Sn_{0.93}Fe_{0.05}Sb_{0.02}O_{2-\sigma}$ (Fe5Sb2) and $Sn_{0.93}Fe_{0.05}Mg_{0.02}O_{2-\sigma}$ (Fe5Mg2) were prepared from stoichiometric SnO_2, Fe_2O_3, Sb_2O_5 and MgO powders via solid-state reaction method. The phase structure of all three samples was investigated by powder X-ray diffraction (XRD, Siemens 5005). High resolution transmission electron microscopy (HRTEM, JEOL-2010F) together with selected area electron diffraction (SAD) and energy dispersive X-ray (EDAX) analysis mapping attachment were used to study the microstructure and doping homogeneity. Magnetic properties were measured by a physical property measurement system (PPMS, Quantum Design) at 300 K. XPS spectra were obtained by a VG ESCALAB 220i-XL instrument with Al Kα monochromatic X-ray source (1486.6 eV). All XPS spectra were calibrated using surface absorbed hydrocarbon at the binding energy of 285.0 eV as a reference.

3. Results and discussion

Fig. 1 shows the XRD results for all samples, demonstrating the pure rutile phase (JCPDS 21-1250). No trace of Fe metal, oxides or other phases was observed in any sample doped up to 5% Fe and 2% M, which is above the detection limit (1%) of our X-ray diffractometer. Lattice parameters (*a*, *c*, cell volume *V*) were determined by Rietveld refinement as shown in Table 1. It can be seen that *a*, *c* and *V* changed in different doping cases. The microstructure and doping homogeneity of sample Fe5Mg2 and Fe5Sb2 were investigated by TEM, as shown in Fig. 2. Fig. 2(b)–(d) gives the typical Sn, Fe and Mg map, respectively, corresponding to the low-magnification TEM image shown in Fig. 2(a). These element mapping results provide the evidence that Fe and Mg have been homogenously distributed in the SnO_2 matrix. The low-magnification TEM image and element mapping results of sample Fe5Sb2 shown in Fig. 2(e)–(h), also demonstrate that the Fe and Sb have been uniformly distributed in the SnO_2 matrix. HRTEM images and SAD patterns of these two samples were carried out to investigate whether Fe clusters or other impurity phases exist, which are suspected to exhibit ferromagnetic ordering. Several arbitrary regions of samples Fe5Sb2 and Fe5Mg2 were investigated by HRTEM. Fig. 2(i) and (j) shows the typical HRTEM results of samples Fe5Sb2 and Fe5Mg2, respectively. No nanocluster or other impurity phase was observed. The SAD patterns corresponding to Fe5Sb2 and Fe5Mg2 shown in Fig. 2(k) and (l), respectively, demonstrated the pure rutile SnO_2 phase. On the other hand, the ionic radii relationship in our samples is: Mg^{2+} (0.72 Å) > Sn^{4+} (0.69 Å) > Sb^{5+} (0.60 Å). Therefore, the Mg^{2+} substitution of Sn^{4+} will increase the lattice volume, whereas Sb^{5+} substitution of Sn^{4+} will decrease the lattice volume. According to the lattice parameters obtained from the XRD results (Table 1), the cell volume indeed increased when doped with Mg and decreased in the case of Sb doping. Based on the above analyses, the Mg and Sb

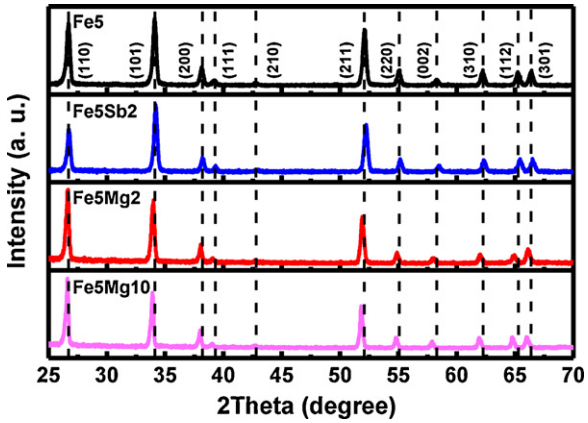

Fig. 1. XRD patterns of the bulk polycrystalline samples of Fe5, Fe5Sb2, Fe5Mg2 and Fe5Mg10.

Table 1
Lattice parameters (a, c), cell volume (*V*), saturation magnetization (M_s), net contribution (Bohr magneton) per Fe ion and Fe^{3+} to Fe^{2+} ratio (Fe^{3+}/Fe^{2+}).

Sample	*a* (Å)	*c* (Å)	*V* (Å^3)	M_s (emu/g)	Contribution per iron (μ_B)	Fe^{3+}/Fe^{2+}
Fe5	4.719 ± 0.002	3.166 ± 0.002	70.5 ± 0.1	0.081 ± 0.001	0.043 ± 0.001	0.83 ± 0.01
Fe5Sb2	4.711 ± 0.002	3.157 ± 0.002	70.0 ± 0.1	0.010 ± 0.001	0.005 ± 0.001	0.53 ± 0.01
Fe5Mg2	4.731 ± 0.002	3.181 ± 0.002	71.2 ± 0.1	0.142 ± 0.001	0.076 ± 0.001	1.28 ± 0.01

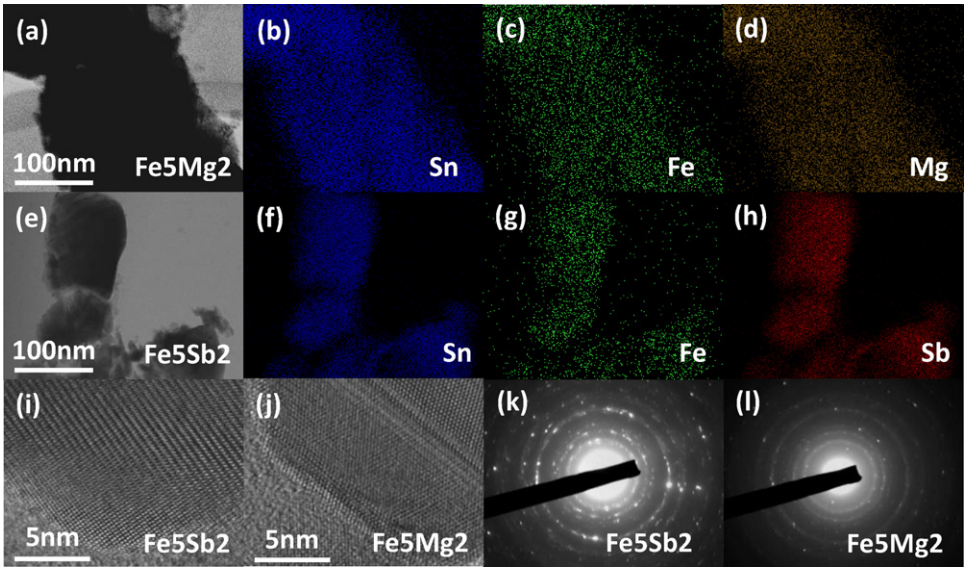

Fig. 2. (a–d) The low-magnification TEM image and its corresponding element mappings of sample Fe5Mg2. (e–h) The low-magnification TEM image and its corresponding element mappings of sample Fe5Sb2. (i and j) The typical HRTEM images of Fe5Sb2 and Fe5Mg2. (k and l) The SAD patterns corresponding to Fe5Sb2 and Fe5Mg2.

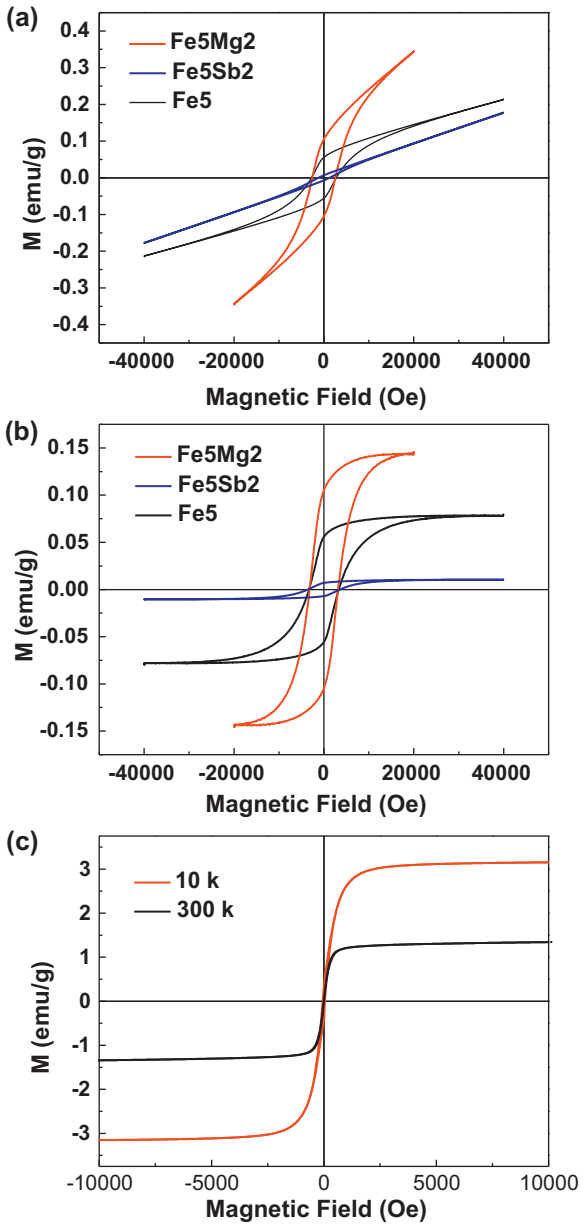

Fig. 3. (a) *M* vs. *H* data of sample Fe5Mg2, Fe5Sb2 and Fe5 measured at 300 K. (b) *M* vs. *H* curve after subtracting the paramagnetic response for the sample Fe5Mg2, Fe5Sb2 and Fe5 measured at 300 K. (c) *M* vs. *H* data of sample Fe5Mg10 measured at 300 K and 10 K.

ions most probably substituted the Sn in the lattice of SnO_2 instead of forming secondary impurity phases.

Fig. 3(a) presents the room-temperature magnetization (*M*, emu/g) vs. magnetic field (*H*, Oe) data of the samples Fe5, Fe5Mg2 and Fe5Sb2, in which a linear component superimposed on a saturating ferromagnetic magnetization is observed. This co-existence of paramagnetic response and ferromagnetic behavior in Fe doped SnO_2 DMS samples has been reported by other groups, and the paramagnetic response was attributed to the Fe ions which are not participating in the ordered magnetic state [23,24]. According to the discussion of Coey et al. [9] and Punnoose et al. [23], these irons did not participate in an ordered magnetic phase, due to: (a) the lack of Fe^{3+} neighbors and/or V_O, (b) the antiferromagnetic exchange interaction of Fe^{3+}–O^{2-}–Fe^{3+}. By subtracting the linear component, the M_s expected for a ferromagnetic phase can be extracted (shown in Fig. 3(b)). The M_s of the three samples are summarized in Table 1. Compared with sample Fe5, the ferromagnetism is found to be strongly suppressed in the electron-doped Fe5Sb2. On the contrary, a significant enhancement of M_s is observed in the hole-doped Fe5Mg2. Although no trace of magnetic impurity phase has been detected in the XRD and TEM characterizations, they may still exist with concentration lower than the detection limits. To further confirm whether the co-doping tuned magnetism in Fe, M co-doped SnO_2 samples originates from doping or is dominated by impurity phases, we increased the hole-doping concentration of Mg to 10% in sample Fe5Mg10 which was fabricated by the same method. Pure SnO_2 rutile phase and the doping induced lattice constants variation can be observed from the XRD results (Fig. 1). The magnetic property of sample Fe5Mg10 was measured at 300 K and 10 K, respectively (Fig. 3(c)). The saturation magnetization at 10 K increased significantly to 3.15 emu/g. By averaging the total magnetization onto 5% Fe dopants, the net contribution from each Fe ions is calculated to be $1.67\mu_B$. It is noteworthy that the net Fe moment in sample Fe5Mg10 is greater than that of any possible magnetic impurity phase; for instance, the net moment per Fe in Fe_3O_4 is $4/3 = 1.33\mu_B$, and that in $MgFe_2O_4$ is $1.1/2 = 0.55\mu_B$ [9,25]. This means that such strong magnetization in Fe5Mg10 cannot be achieved, even if all the doped irons exist as magnetic impurity phases instead of substitutions in the SnO_2 lattice. On the other hand, the XRD results indicate that the impurity phase concentration should be lower than the detection limit (~1%). Based on the above analyses, it is evidenced that the ferromagnetism in our Fe, M co-doped SnO_2 samples cannot be simply attributed to the impurity phases.

Considering that the ferromagnetism in Fe-doped SnO_2 originates from the spin of Fe ions and their exchange interactions, the oxidation state of Fe should be directly related to the magnetic properties of our $Sn_{0.93}Fe_{0.05}M_{0.02}O_{2-\sigma}$ [9,20]. In order to investigate the oxidation state of Fe ions, high-resolution Fe 2p core level spectra of the samples Fe5, Fe5Sb2 and Fe5Mg2 were recorded and shown in Fig. 4(a). Fitting of the asymmetric core lines into four Voiget components together with Shirley background gives a good description of the overall core line shape. The peaks located around 711.1 eV and 713.7 eV are assigned to the Fe^{2+} and Fe^{3+}, respectively. The Sn 3p peak (716.5 eV) is also observed since its binding energy is very close to the Fe 2p. The peak with highest binding energy in the spectra corresponds to the Fe 2p satellite. From these XPS results, we can see that both Fe^{3+} and Fe^{2+} co-exist in all three samples. By calculating the peak area ratio of Fe^{3+} to Fe^{2+}, the relative concentration of Fe^{3+} and Fe^{2+} was estimated and the results are shown in Table 1. It is interesting to note that, compared with sample Fe5, the sample Fe5Sb2 has lower Fe^{3+} intensity while Mg doping leads to more Fe^{3+} in sample Fe5Mg2. This variation of Fe oxidation state can be understood in terms of its compensation effect to the charge imbalance arising from the substitution of Sn^{4+} by Mg^{2+} and Sb^{5+}. Since the spin state of Fe^{3+} is higher than Fe^{2+}, the enhancement of M_s in Fe5Mg2 and decrease in Fe5Sb2, which were revealed in *M*–*H* measurements can be attributed to this doping induced variation of Fe oxidation state.

On the other hand, the carriers are found to play a critical role in the ferromagnetic exchange of DMS [19,21,22]. According to the defect Eqs. (1) and (2), the role of Sb and Mg in SnO_2 is donor and acceptor, respectively. To experimentally determine the carrier type for the Mg and Sb doping, we further carried out the XPS valence band (VB) measurement. Fig. 4(b) presents the VB spectra for all the three samples. In semiconductor materials, the Fermi level (E_f) will shift towards the valence band maximum (VBM) in p-type doping and be away from VBM in the case of n-type doping. Accordingly, the doping type can be determined by studying the relative position between E_f and VBM [26–28]. The XPS VB spectrum is a powerful technique to get the information of E_f and VB, in which E_f is located at 0 eV and the VBM with respect to the E_f can be deter-

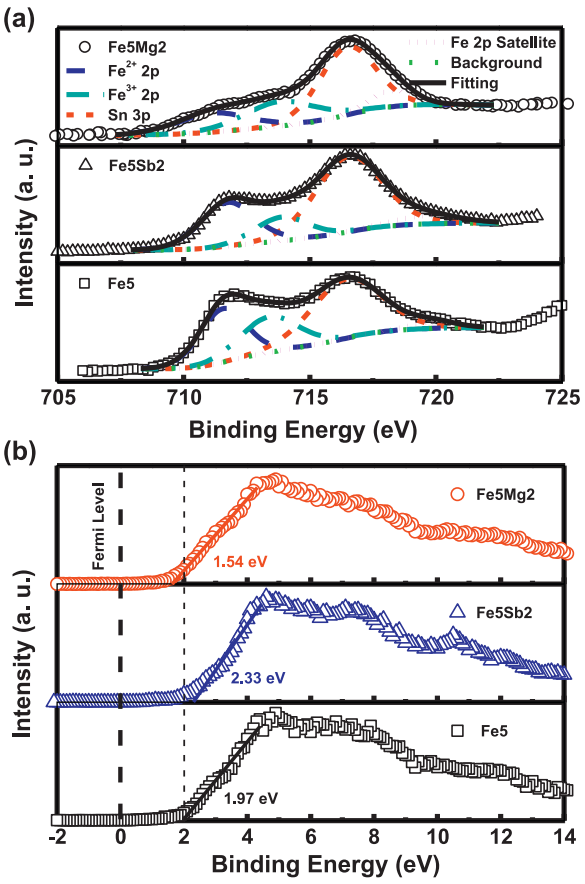

Fig. 4. (a) Core-level Fe 2p XPS spectra of sample Fe5Mg2, Fe5Sb2 and Fe5. The spectra were fitted to a Shirley background (green dot line) together with the Voigt profiles for Fe^{2+} (dash line), Fe^{3+} (dash dot line), Sn 3p (dash line) and Fe 2p satellite (short dot line). The fitting curves (solid line) are seen to match well with the experimental data points. (b) Valence band spectra of the sample Fe5Mg2, Fg5Sb2 and Fe5. (For interpretation of the references to color in this figure legend, the reader is referred to the web version of the article.)

mined by extrapolating the leading edge of the VB to its intersection with the background. According to VB spectra shown in Fig. 4(b), the E_f of sample Fe5Sb2 shifts away from the VBM, compared with sample Fe5. In the case of Mg doping (sample Fe5Mg2), the E_f moves toward the VBM. As a result, electron-doping of Sb and hole-doping of Mg in $Sn_{0.93}Fe_{0.05}M_{0.02}O_{2-\sigma}$ are confirmed. Referring to the *M–H* results, the ferromagnetism in $Sn_{0.93}Fe_{0.05}M_{0.02}O_{2-\sigma}$ is found to be enhanced by hole-doping and destroyed by electron-doping.

4. Conclusions

In conclusion, the doping effects of Sb and Mg on the ferromagnetic properties of $Sn_{0.93}Fe_{0.05}M_{0.02}O_{2-\sigma}$ were investigated. XPS results demonstrate that the concentration of high spin state Fe ions (Fe^{3+}) increased in the hole (Mg)-doped sample while decreased in the case of electron (Sb)-doping. The doping type of Mg and Sb in $Sn_{0.93}Fe_{0.05}M_{0.02}O_{2-\sigma}$ was confirmed by XPS VB measurements. The change of Fe oxidation state and variation of carrier type are believed to be responsible for the co-doping tuned ferromagnetism in $Sn_{0.93}Fe_{0.05}M_{0.02}O_{2-\sigma}$.

Acknowledgement

The grant support of Singapore A*STAR SERC Grant no: 102 101 0019 for this work is acknowledged.

References

[1] S.B. Ogale, Adv. Mater. 22 (2010) 3125–3155.
[2] R.K. Singhal, A. Samariya, Y.T. Xing, S. Kumar, S.N. Dolia, U.P. Deshpande, T. Shripathi, E.B. Saitovitch, J. Alloys Compd. 496 (2010) 324–330.
[3] Y. Wang, F.X. Xiu, X.F. Kou, A.P. Jacob, K.L. Wang, J. Zou, J. Alloys Compd. 508 (2010) 273–277.
[4] J.X. Deng, Y.F. Tian, S.S. Yan, Q. Cao, G.L. Liu, Y.X. Chen, L.M. Mei, G. Ji, Z. Zhang, J. Appl. Phys. 104 (2008) 013905.
[5] J.X. Deng, Y.F. Tian, S.M. He, H.L. Bai, T.S. Xu, S.S. Yan, Y.Y. Dai, Y.X. Chen, G.L. Liu, L.M. Mei, Appl. Phys. Lett. 95 (2009) 062513.
[6] S.R. Dunsiger, J.P. Carlo, T. Goko, G. Nieuwenhuys, T. Prokscha, A. Suter, E. Morenzoni, D. Chiba, Y. Nishitani, T. Tanikawa, F. Matsukura, H. Ohno, J. Ohe, S. Maekawa, Y.J. Uemura, Nat. Mater. 9 (2010) 299–303.
[7] W. Yan, Z. Sun, Z. Pan, Q. Liu, T. Yao, Z. Wu, C. Song, F. Zeng, Y. Xie, T. Hu, S. Wei, Appl. Phys. Lett. 94 (2009) 042508.
[8] J. Wan, Q. Lu, B. Chen, F. Song, J. Liu, J. Dong, G. Wang, Appl. Phys. Lett. 95 (2009) 152901.
[9] J.M.D. Coey, A.P. Douvalis, C.B. Fitzgerald, M. Venkatesan, Appl. Phys. Lett. 84 (2004) 1332.
[10] D. Mukherjee, T. Dhakal, H. Srikanth, P. Mukherjee, S. Witanachchi, Phys. Rev. B 81 (2010) 205202.
[11] M.L. Dinesha, H.S. Jayanna, S. Mohanty, S. Ravi, J. Alloys Compd. 490 (2010) 618–623.
[12] X.Y. Xu, C.B. Cao, J. Alloys Compd. 501 (2010) 265–268.
[13] X.J. Lue, J.T. Li, X.L. Mou, J.J. Wu, S.J. Ding, F.Q. Huang, Y.M. Wang, F.F. Xu, J. Alloys Compd. 499 (2010) 160–165.
[14] N.H. Hong, J. Sakai, N. Poirot, V. Brizé, Phys. Rev. B 73 (2006) 132404.
[15] J.M.D. Coey, P. Stamenov, R.D. Gunning, M. Venkatesan, K. Paul, New J. Phys. 12 (2010) 053025.
[16] S. Zhou, E. Čižmár, K. Potzger, M. Krause, G. Talut, M. Helm, J. Fassbender, S.A. Zvyagin, J. Wosnitza, H. Schmidt, Phys. Rev. B 79 (2009) 113201.
[17] J.M.D. Coey, M. Venkatesan, C.B. Fitzgerald, Nat. Mater. 4 (2005) 173–179.
[18] X.J. Liu, X.Y. Zhu, J.T. Luo, F. Zeng, F. Pan, J. Alloys Compd. 482 (2009) 224–228.
[19] S.C. Li, P. Ren, B.C. Zhao, B. Xia, L. Wang, Appl. Phys. Lett. 95 (2009) 102101.
[20] A. Thurber, K.M. Reddy, A. Punnoose, J. Appl. Phys. 105 (2009) 07E706.
[21] D. Karmakar, S.K. Mandal, R.M. Kadam, P.L. Paulose, A.K. Rajarajan, T.K. Nath, A.K. Das, I. Dasgupta, G.P. Das, Phys. Rev. B 75 (2007) 144404.
[22] Y.H. Lin, J.N. Cai, C.W. Nan, M. Kobayashi, J.L. He, J. Appl. Phys. 99 (2006) 056107.
[23] A. Punnoose, J. Hays, A. Thurber, M.H. Engelhard, R.K. Kukkadapu, C. Wang, V. Shutthanandan, S. Thevuthasan, Phys. Rev. B 72 (2005) 054402.
[24] J.F. Liu, M.F. Lu, P. Chai, L. Fu, Z.L. Wang, X.Q. Cao, J. Meng, J. Magn. Magn. Mater. 317 (2007) 1–7.
[25] A. Goldman, Handbook of Modern Ferromagnetic Materials, Kluwer Academic Publisher, Norwell, 1999 (Chapter 11).
[26] S.S. Lin, J.I. Hong, J.H. Song, Y. Zhu, H.P. He, Z. Xu, Y.G. Wei, Y. Ding, R.L. Snyder, Z.L. Wang, Nano Lett. 9 (2009) 3877–3882.
[27] Z.Z. Ye, Y.J. Zeng, Y.F. Lu, S.S. Lin, L. Sun, L.P. Zhu, B.H. Zhao, Appl. Phys. Lett. 91 (2007) 112110.
[28] G. Hesong, X. Xia, Y. Zhang, F. Gao, W. Li, G. Wu, X. Li, G. Du, J. Phys. Condens. Matter 20 (2008) 292202.